Acta Pharmaceutica Sinica B 2024;14(11):4883–4898

Chinese Pharmaceutical Association
Institute of Materia Medica, Chinese Academy of Medical Sciences

Acta Pharmaceutica Sinica B

www.elsevier.com/locate/apsb
www.sciencedirect.com

ORIGINAL ARTICLE

Adipose ADM2 ameliorates NAFLD *via* promotion of ceramide catabolism

Pengcheng Wang[a,†], Song-Yang Zhang[d,†], YongQiang Dong[c,†], Guangyi Zeng[d], Huiying Liu[d], Xian Wang[d], Changtao Jiang[a,b,d,*], Yin Li[d,e,*]

[a]*Center of Basic Medical Research, Institute of Medical Innovation and Research, Third Hospital, Peking University, Beijing 100191, China*
[b]*Department of Immunology, School of Basic Medical Sciences, NHC Key Laboratory of Medical Immunology, Peking University, Beijing 100191, China*
[c]*The First Affiliated Hospital of Zhengzhou University, Zhengzhou University, Zhengzhou 450052, China*
[d]*Department of Physiology and Pathophysiology, School of Basic Medical Sciences, Peking University, State Key Laboratory of Vascular Homeostasis and Remodeling, Beijing 100191, China*
[e]*Department of Integration of Chinese and Western Medicine, School of Basic Medical Sciences, Peking University; Tasly Microcirculation Research Center, Peking University Health Science Center, Beijing 100191, China*

Received 7 February 2024; received in revised form 25 June 2024; accepted 15 July 2024

KEY WORDS

Non-alcoholic fatty liver disease;
Adipose tissue;
Lipid metabolism;
Adrenomedullin 2;
Ceramide;
HIF2α;
ACER2

Abstract The adipose tissue of mammals represents an important energy-storing and endocrine organ, and its dysfunction is relevant to the onset of several health problems, including non-alcoholic fatty liver disease (NAFLD). However, whether treatments targeting adipose dysfunction could alleviate NAFLD has not been well-studied. Adrenomedullin 2 (ADM2), belonging to the CGRP superfamily, is a protective peptide that has been shown to inhibit adipose dysfunction. To investigate the adipose tissue-specific effects of ADM2 on NAFLD, adipose-specific ADM2-overexpressing transgenic (aADM2-tg) mice were developed. When fed a high-fat diet, aADM2-tg mice displayed decreased hepatic triglyceride accumulation compared to wild-type mice, which was attributable to the inhibition of hepatic *de novo* lipogenesis. Results from lipidomics studies showed that ADM2 decreased ceramide levels in adipocytes through the upregulation of ACER2, which catalyzes ceramide catabolism. Mechanically, activation of adipocyte HIF2α was required for ADM2 to promote ACER2-dependent adipose ceramide catabolism as well as to decrease hepatic lipid accumulation. This study highlights the role of ADM2 and adipose-derived ceramide in NAFLD and suggests that its therapeutic targeting could alleviate disease symptoms.

*Corresponding authors.
E-mail addresses: jiangchangtao@bjmu.edu.cn (Changtao Jiang), yinli@bjmu.edu.cn (Yin Li).
†These authors made equal contributions to this work.
Peer review under the responsibility of Chinese Pharmaceutical Association and Institute of Materia Medica, Chinese Academy of Medical Sciences.

https://doi.org/10.1016/j.apsb.2024.09.010

1. Introduction

Non-alcoholic fatty liver disease (NAFLD), characterized by increased hepatic lipid accumulation, is the most common liver disease worldwide[1,2]. There has been a rising trend in the prevalence of NAFLD, paralleled with a worldwide increase in metabolic syndrome, ranging from simple fatty liver to more severe non-alcoholic steatohepatitis (NASH)[3,4]. In Asia, the risk factors of NAFLD progression include sedentary lifestyle, diet, genetics, aging, diabetes, insulin resistance, and obesity[5-7]. Unfortunately, the pharmacological therapies against NAFLD are still limited to date[8].

Fatty liver, marked by the increased triglyceride deposition in the liver, reflects an input/output imbalance of hepatic free fatty acids. The adipose tissue of mammals is well-recognized collectively as an organ for lipid storage[9], and its dysfunction is linked to NAFLD. In clinical studies involving MRI and liver biopsy in humans, liver inflammation and fibrosis are positively associated with visceral adipose mass[10,11]. The secretion of lipids, adipokines, and proinflammatory cytokines from adipocytes, and adipose macrophage infiltration have been shown to collectively contribute to the onset of NASH[4], which makes the communication between adipose tissue and the liver a crucial area of investigation. Thus, exploring their interaction will facilitate the understanding of NAFLD onset.

As a group of sphingolipid species, ceramides are synthesized from three different pathways: *de novo* synthesis, sphingomyelin hydrolysis, and salvage pathways[12,13]. The ceramides are generated from the various synthesizing pathways under different physiological and pathophysiological conditions, while ceramide overproduction during this process causes lipotoxicity, endoplasmic reticulum/mitochondrial stress, inflammation, and dysregulation of hepatic lipid metabolism[12,14]. Additionally, ceramide can also promote NAFLD indirectly through induction of dyslipidemia, given its actions in promoting lipid synthesis and very low-density lipoprotein secretion within the liver[15-17]. In studies with rodents, inhibition of ceramide biosynthesis or activation of ceramide degradation ameliorates insulin resistance, atherosclerosis, and steatohepatitis[13,14,18-20].

Adrenomedullin 2 (ADM2), also known as intermedin (IMD), is an endogenous peptide that belongs to the calcitonin gene-related peptide (CGRP) superfamily. The ADM2 gene is located in the distal 22q13.33 region of the long arm of human chromosome 22 and encodes a pre-secretory peptide containing 148 amino acid residues[21]. The members of CGRP) superfamily have a conserved molecular structure, a disulfide ring structure composed of 6 amino acid residues[22]. Calcitonin receptor and calcitonin receptor-like receptor (CRLR) are G protein-coupled receptors (GPCRs) shared by members of the CGRP superfamily. Previous results have shown that ADM2 can activate downstream signals of CRLR, but cannot activate downstream signals of CT, indicating that CRLR is an endogenous receptor of ADM2[23]. Recently, Babin's group reported that Adrenomedullin 2/intermedin is a slow off-rate, long-acting endogenous agonist of the adrenomedullin$_2$ G protein-coupled receptor[24]. ADM2 is widely expressed throughout the body, including in the adipose tissue, kidneys, intestine, colon, rectum, and ovaries, and it is especially highly expressed in the circulatory system. However, plasma levels of ADM2 are relatively low[25], indicating that ADM2 may act in an autocrine or paracrine manner, regulating organ perfusion and hormone secretion[22]. Previous studies, including by our group, have reported that ADM2 treatment reduces atherosclerosis by inhibiting foam cell formation and improving dyslipidemia[26,27], and enhances beiging of white adipose tissue directly in an adipocyte-autonomous manner and indirectly through M2 macrophage polarization[28]. ADM2 has functions in the cardiovascular, lymphatic, and nervous systems by activating three heterodimeric receptors comprising the class B GPCR CLR and a RAMP-1, -2, or -3 modulatory subunit[24]. ADM2 has positive inotropic and positive inotropic effects in Mianyang and rats[29]. ADM2 can directly enhance myocardial contractility by increasing intracellular calcium concentration in a PKA and PKC-dependent manner[30]. However, whether ADM2 has a protective effect on NAFLD development is still unknown.

ADM2 is expressed in the adipose tissue and is downregulated during obesity in mice[31]. The plasma level of ADM2 is negatively associated with the body mass index and HOMA-IR index in humans, indicating that ADM2 may inhibit metabolic syndrome by targeting the adipose tissue. Moreover, elevated adipocyte-derived ceramide and ectopic lipid deposition are very important pathogenic factors. It is important to search for local interventions with endogenous factors within the adipose tissue, and further investigate how they inhibit molecular mechanisms. Herein, we have utilized adipose-specific ADM2 transgenic (aADM2-tg) mice to study the role and dissect the mechanisms of ADM2 in adipose ceramide generation and NAFLD development. Our results suggest that the activation of adipocyte HIF2α is required for ADM2 induction. Mechanistically, we found that adipocyte ADM2-activated HIF2α ameliorated NAFLD by activating ceramide catabolism. Particularly, *Acer2*, encoding a key enzyme that hydrolyzes ceramides to sphingosines and free fatty acids in alkaline conditions, and which was confirmed as the target gene of HIF2α[18], was significantly activated. This study highlights the role of ADM2 and adipose-derived ceramide in NAFLD and provides a new strategy and potential drug candidate for the treatment of NAFLD.

2. Materials and methods

2.1. Animals

The transgenic mouse line with adipocyte-specific overexpression of the *ADM2* gene (aADM2-tg mice) was generated on a C57BL/6J background with the human *ADM2* gene driven by the adiponectin (Adipoq) gene promoter (H11-Adipoq-hADM2-Wpre-PolyA mice, Strain No. T059304). The mice were purchased from GemPharmatech (Nanjing, China) as described previously[28,32]. *Hif2a*$^{fl/fl}$ mice were previously described[18]. To achieve adipocyte-specific disruption, *Hif2a*$^{fl/fl}$ mice were crossed with mice harboring Cre-recombinase under the control of the adiponectin promoter to obtain *Hif2a*$^{\Delta Adipo}$ mice[12,33]. 8−10 weeks male aADM2-tg(+/+) and their WT littermates(−/−) mice, *Hif2a*$^{\Delta Adipo}$

and *Hif2a*$^{fl/fl}$ mice were housed with a 12-h light/dark cycle. Animals were fed *ad libitum* with either a chow diet or a high-fat diet (D12492, Research Diets). Surgery and implantation of osmotic minipumps: As previously reported[34], mice were anesthetized with isoflurane. A 1-cm incision was made in the back skin and mice were implanted subcutaneous injection with an Alzet osmotic minipump (model 1002) filled with vehicle or ADM2. Before implantation, the pumps were filled with a test agent and then placed in a Petri dish with sterile 0.9% saline (NS) at 37 °C for at least 4 h before implantation to prime the pumps. For the knockdown experiment of the *Acer2* gene, the Acer2-shRNA sequence (shRNA_ID:*Acer2*.3550: 5′-ACAGTGTTGTGTTGAGGATCAA-3′) was cloned into LV-miRE-EGFP vector. Lentivirus was produced in HEK293T cells and concentrated by ultracentrifugation at 25,000 rpm for 2.5 h. Eight-week-old aADM2-tg mice were administered with recombinant lentivirus expressing Lenti-Sh*Acer2 or* Vector into the epididymal fat pad of the mice (1×10^7 infection unit per mouse), respectively, as previously reported[15]. All mice were randomly assigned to experimental groups, and the groups did not present any differences in body weights before the treatments. All mice were housed within a SPF facility and no mice were excluded from the analysis. All animal experiments were approved by the Animal Research Ethics Committees.

2.2. Materials

Human adrenomedullin2/intermedin (ADM2) and ADM2 antibody were from Phoenix Pharmaceuticals (Belmont, CA, USA). The anti-F4/80 (D2S9R) (Cat#70076S, RRID: AB_2799771), the anti-Histone H2A.X (Cat#7631, RRID: AB_10860771), the anti-ATGL (Cat#2138, RRID: AB_2167955), anti-HSL (Cat#4107, RRID: AB_2296900), and anti-phospho HSL (Ser660) (Cat#4126, RRID: AB_490997) were purchased from Cell Signaling (Danvers, MA, USA). The anti-ACER2 rabbit polyclonal antibody (Cat#PA5-39016; RRID: AB_2555608) was purchased from Invitrogen (CA, USA). The anti-HIF2α rabbit polyclonal antibody (Cat# NB100-122; RRID: AB_10002593) was purchased from Novus (CO, USA). The anti-HIF1α rabbit polyclonal antibody (Cat#20960-1-AP, RRID: AB_10732601) was purchased from Proteintech (Rosemont, IL, USA). The anti-β-actin mouse monoclonal antibody (Cat#A3854, RRID: AB_262011) and peroxidase-conjugated goat anti-mouse IgG (Cat#A4416, RRID: AB_258167) were purchased from Sigma−Aldrich (St. Louis, MO, USA), and the peroxidase-conjugated goat anti-rabbit IgG (Cat#ZB2301, RRID: AB_2747412) was purchased from Zhongshan Golden Bridge Biotechnology (Beijing, China).

2.3. Cell culture

2.3.1. Isolation and culture of primary adipocytes

As previously reported[35], mature adipocytes were isolated from epididymal fat pads of C57BL/6 mice aged 6−8 weeks. The epididymal fat pads were minced and incubated at 37 °C for 1 h in 1 mg/mL type I collagenase. Packed adipocytes were washed for twice and diluted in serum-free Dulbecco's modified Eagle's medium (DMEM) to generate a 10% (*v*/*v*) cell suspension.

2.3.2. Isolation and culture of primary hepatocytes

As previously reported[36], mice were anesthetized with 1% Nembutal (7 μL/g body weight) and injected intraperitoneally with 1000 IU heparin. After laparotomy, the portal vein was cannulated. The liver was perfused with 20 mL pre-warmed D-Hanks buffer, followed by 20 mL of 0.02% collagenase (Sigma−Aldrich, St. Louis, MO, USA) at a flow rate of 2 mL/min. After perfusion, liver tissues were removed and washed with 20 mL D-Hanks Buffer. The capsule of the liver was removed, and hepatic tissues dispersed and incubated in 20 mL of 0.01% collagenase in a shaking water bath for 15 min. The cell suspension was then filtered through two layers of 70 μm nylon mesh, centrifuged at 500 rpm, and washed twice with DMEM to remove tissue dissociation enzymes, damaged cells, and non-parenchymal cells. Dispersed hepatocytes were counted and seeded at a concentration of 10^5 cells/100 mm dish, containing 10 mL high glucose DMEM supplemented with 10% FBS. Cells were cultured at 37 °C in a humidified atmosphere of 5% CO_2. The culture medium was changed daily.

2.3.3. Culture and differentiation of 3T3-L1 cells

As previously reported[37], 3T3-L1 cells (American Type Culture Collection) were cultured in growth medium, high-glucose DMEM, supplemented with 10% FBS, 100 units/mL penicillin, and 100 units/mL streptomycin. Two days post−confluence, cells were induced to differentiate with a standard cocktail consisting of a growth medium with 1 mmol/L dexamethasone, 10 mg/mL bovine insulin, and 0.25 mmol/L 3-isobutyl-1-methylxanthine. After 3 days in the differentiation medium, the cells were treated with a growth medium containing 10 mg/mL bovine insulin for 3 days and then maintained in a growth medium alone. Cells were considered mature adipocytes 8 days after the induction of differentiation.

2.4. Histology

Fresh tissues were excised, fixed in 4% paraformaldehyde, and paraffin-embedded. Sections were stained with H&E. Histological scoring for liver NAFLD was read blinded to the experimental design using H&E staining. The degree of steatosis, ballooning, and lobular inflammation was evaluated according to previously published criteria based on the conclusions of the American Association for the Study of Liver Disease (AASLD)[38]. The NAS consists of the sum of steatosis, ballooning, and lobular inflammation. For Oil Red O staining, 7 μm cryosections were prepared on O.C.T-embedded frozen liver sections. Slides were fixed in 4% (*v*/*v*) paraformaldehyde for 1 h, rinsed in ddH_2O, and stained for 15 min in freshly prepared Oil Red O in 60% isopropanol.

2.5. Immunofluorescence and immunohistochemistry

For immunofluorescence, as previously reported[35], primary hepatocytes and adipocytes mice were was fixed in 4% paraformaldehyde for 10 min, the cells were blocked in 1% BSA in PBS for 1 h at room temperature. They were then washed in 1× PBS/0.1% Tween-20 three times for 5 min each. And then incubated overnight at 4 °C with antibodies accordingly. They were then washed in 1X PBS/0.1% Tween-20 three times for 5 min each. Cells were then incubated at room temperature for 1 h with the secondary antibodies. The nuclei were visualized by staining with Hoechst 33258 for 10 min. The lipid droplets were visualized by staining with Lipidtox deep green (Invitrogen-H34475) for 10 min. Photomicrographs were taken under a confocal laser-scanning microscope (Leica, Germany). For immunohistochemistry, the tissue was fixed in 4% paraformaldehyde, dehydrated, embedded in wax, and sectioned at 7 μm. Paraffin-embedded sections were de-waxed, re-hydrated, and rinsed in PBS. After

boiling for 10 min in 10 mmol/L sodium citrate buffer (pH 6.0), the sections were blocked in 1% BSA in PBS for 1 h at room temperature, then incubated overnight at 4 °C with antibodies accordingly. They were then washed in 1 × PBS/0.1% Tween-20 three times for 5 min each. Tissue sections were then incubated at room temperature for 1 h with the secondary antibodies. And then proceed with the substrate reaction according to the instructions.

2.6. *Biochemical and immunological assays*

Plasma ALT, AST, cholesterol, and triglyceride levels were quantified using commercial kits (BioSino Bio-Technology and Science, Beijing, China) according to previous protocols[18]. Approximately 20 mg of liver tissue was accurately weighed, homogenized in triglyceride cracking liquid, and centrifuged at 2,000 rpm for 5 min at 4 °C. The supernatant was collected to quantify hepatic cholesterol and triglyceride levels. Hepatic total cholesterol and triglyceride concentrations were quantified, normalized to the corresponding weight, and then expressed as milligrams of lipid per gram of tissue weight.

2.7. *qPCR and RNA-Seq profiling*

Total RNA from tissues or cells was isolated using TRIzol (Invitrogen, Darmstadt, Germany), following the manufacturer's instructions. One μg of RNA was reverse-transcribed using a 5 × All in one RT MasterMix (Cat# G490, AMB), and real-time PCR was performed. Calculation normalization was performed to 18s RNA. One μg of total RNA was used for library preparation. The poly(A) mRNA isolation was performed using Oligo(dT) beads. Then libraries with different indexes were multiplexed and loaded on an Illumina HiSeq/Illumina Novaseq/MGI2000 instrument for sequencing using a 2 × 150 paired-end (PE) configuration according to the manufacturer's instructions.

2.8. *Western blotting analysis*

The adipose tissues and liver were lysed in RIPA buffer with protease and phosphatase inhibitors, and then the protein extracts were resolved by SDS−PAGE electrophoresis and transferred onto polyvinylidene difluoride (PVDF) membranes. Membranes were blocked with 5% skimmed milk for 1 h at room temperature and then incubated with primary antibodies and HRP-conjugated secondary antibodies. The blots were visualized with chemiluminescence, and the densitometry of the blots was detected using a LI-COR Odyssey Fc imager (LI-COR Biosciences, Lincoln, NE, USA).

2.9. *Metabolomics analysis*

Lipidomics analysis was performed according to previously published protocols[18]. For the plasma lipidomics analysis, 50 μL of serum was extracted with 200 μL of cold chloroform: methanol (2:1) solution containing 1 μmol/L LM6002 (Avanti Polar Lipids, Alabaster, AL) as the internal standard. For the lipidomics analysis of adipose tissue, approximately 20 mg of adipose tissue was homogenized with 200 μL of H_2O and then extracted with 1000 mL of cold chloroform: methanol (2:1) solution containing 1 μmol/L LM6002 (Avanti Polar Lipids, Alabaster, AL, USA) as an internal standard. After vortexing for 1 min, the sample was incubated at room temperature for 30 min and subsequently centrifuged at 13,000 rpm for 20 min at 4 °C. The lower organic phase was collected and evaporated. The organic residue was dissolved in 50 mL of isopropanol: acetonitrile (1:1) solution. Samples were analyzed by Eksigent LC100 coupled with AB SCIEX Triple TOF 5600 system. All of the lipid molecules were identified through the acknowledged database Lipidmaps (http://www.lipidmaps.org) and the comparison with the standards (including retention time, parent ion mass, and MS/MS fragmentations). Peak extraction and integration were performed with PeakView1.2 software (AB SCIEX, Washington D.C., USA). Partial least squares discriminant analysis (PLS-DA) and variable importance for the projection (VIP) score were carried out using MetaboAnalyst 6.0 (http://www.metaboanalyst.ca). For quantitation of sphingolipid metabolites, the data was analyzed by MultiQuant2.1 software (AB SCIEX, Washington D.C., USA).

2.10. *Bioinformatics analysis*

For RNA-Seq data analysis, raw reads were filtered to include only those with a median Phred quality score of $\geq$20 and trimmed with cutadapt v1.9.1 to remove adapter sequences. RNA-Seq reads were subsequently aligned to the mouse reference genome (version mm9) using subread 1.5.1 with default parameters. Unique reads were kept and annotated to RefSeq genes using featureCounts. Only genes with an FPKM value of $\geq$0.1 in all samples were kept for downstream analysis. Differential expression analysis was performed using limma and determined using a cutoff significance level of FDR $<$0.05. Functional enrichment analysis was performed with DAVID using the pathways related to metabolism from the KEGG database annotation[39,40]. RNA-Seq datasets are available for download from the Sequence Archive with accession number GSE267858.

2.11. *Statistical analyses*

The data were analyzed using GraphPad Prism 9.0 software (GraphPad Software, San Diego, CA, USA) and IBM SPSS 24.0 (IBM Corporation, Armonk, NY). Data are expressed as mean ± standard error of mean (SEM) and statistically analyzed by Student's *t*-test, or Mann−Whitney U as appropriate, and one-way ANOVA with Tukey's *post hoc* test. Significance was set at $P < 0.05$. P values are presented in the indicated figures.

3. Results

3.1. *Adipose ADM2 improves NAFLD independent of adipocyte lipolysis*

To determine the effect of adipose ADM2 on NAFLD, wild-type (WT) and aADM2-tg mice were challenged with a high-fat diet (HFD) for 8 weeks. The decreased accumulation of lipid in the liver was observed in aADM2-tg mice *via* oil red O and H&E stainings of liver sections (Fig. 1A). Furthermore, histological assessment showed that aADM2-tg mice displayed improved steatosis, ballooning, inflammation, as well as a lower NAFLD Activity Score (NAS) (Fig. 1B−E). The liver and body weight ratios were decreased in aADM2-tg mice (Fig. 1F). The mRNA and protein levels of *Adm2* were specifically increased in the white adipose tissue (WAT) of aADM2-tg mice, with no changes in macrophages, liver, and skeletal muscle (Supporting Information

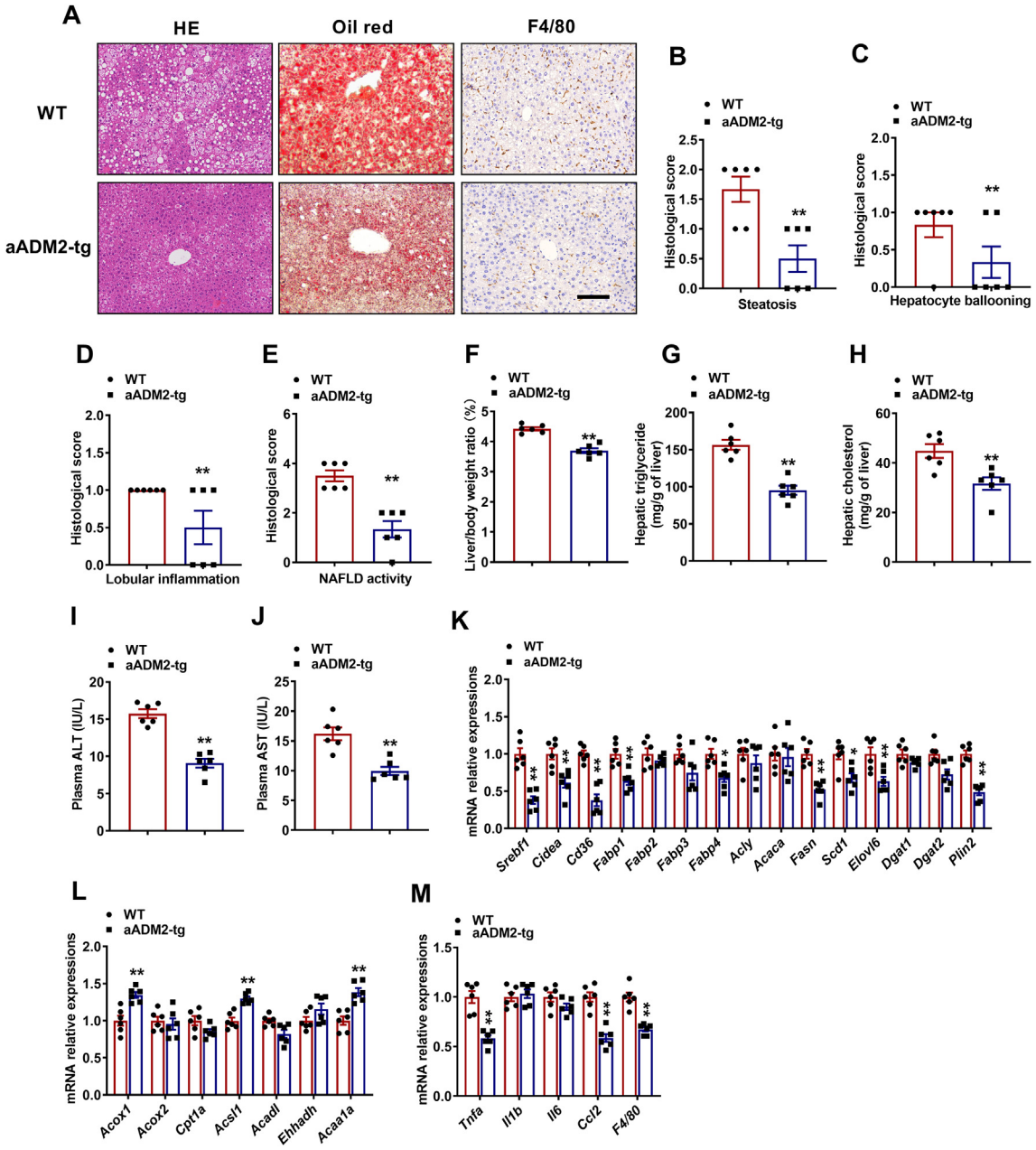

Figure 1 Adipose ADM2 improves NAFLD. WT and aADM2-tg mice were fed an HFD for 8 weeks. (A) H&E, oil red O staining and F4/80 markers of representative liver sections ($n = 6$), Scale bars, 100 μm. (B) Histological scoring for steatosis ($n = 6$). (C) Histological scoring for hepatocellular ballooning ($n = 6$). (D) Histological scoring for hepatocellular inflammation ($n = 6$). (E) Histological scoring ($n = 4$). (F) Liver and body weight ratio of mice ($n = 6$). (G) Hepatic triglyceride content of mice ($n = 6$). (H) Hepatic total cholesterol content of mice ($n = 6$). (I) Plasma level of ALT ($n = 6$). (J) Plasma level of AST ($n = 6$). (K) Hepatic expression of mRNAs encoded by hepatic fatty acid transport and lipogenesis-related genes. (L) Hepatic expression of mRNAs encoded by hepatic fatty acid β-oxidation-related genes. (M) Hepatic expression of mRNAs encoded by inflammatory cytokine and chemokine genes. All data are presented as the mean ± SEM. Two-tailed Student's *t*-test (G−K, M) and Mann−Whitney U test (B−F, L): $^{*}P < 0.05$, $^{**}P < 0.01$ compared to the WT mice.

Fig. S1A and S1B). No significant increase in plasma ADM2 level was observed in aADM2-tg mice (Fig. S1C), which excluded the mechanism of a direct action of adipose ADM2 on the liver through an endocrine manner. The body weight of aADM2-tg mice was decreased compared to controls (Fig. S1D), while the food intake was not altered (Fig. S1E), which is consistent with our previous report that adipose ADM2 protected against HFD-induced obesity[31].

Next, the hepatic lipid contents in the WT and aADM2-tg mice were examined further. Compared to controls, the hepatic triglyceride and total cholesterol contents were decreased in aADM2-tg mice (Fig. 1G and H). The plasma levels of ALT and AST were also decreased in samples from aADM2-tg mice (Fig. 1I and J), indicating improved hepatic function. The plasma levels of triglyceride and total cholesterol were also decreased in aADM2-tg mice (Fig. S1F and S1G). Furthermore, the mRNA

expression of genes involved in fatty acid transport and anabolism (*Srebp1*, *Cidea*, *Cd36*, *Fabp1*, *Fabp4*, *Fasn*, *Scd1*, and *Elovl6*), triglyceride synthesis (*Dgat2*), and the lipid-droplet coat (*Plin2*) were all substantially reduced in aADM2-tg mice, compared to controls (Fig. 1K). By contrast, the mRNA expression of genes involved in fatty acid β-oxidation, such as *Acox1*, *Acsl1*, and *Acaa1a*, were moderately elevated in aADM2-tg mice compared to control mice (Fig. 1L). Moreover, the expression levels of inflammatory cytokines, such as *Tnfa*, *Ccl2,* and *F4/80*, were significantly lower in aADM2-tg mice compared to control mice (Fig. 1M). Consistent with this, the immunohistochemical staining of liver slices also showed a significant reduction in F4/80 positive cells, a macrophage infiltration marker, in the liver (Fig. 1A). The hepatic and plasma levels of glycerol and NEFA were not changed in aADM2-tg mice (Fig. S1H−S1K). The expression levels of adipose lipolysis genes, *Atgl*, *Hsl*, *Mgl*, and *Perilipin*, and the expression of ATGL and HSL phosphorylation protein levels, remain unchanged (Fig. S1L and S1M), indicating that ADM2 does not affect adipocyte lipolysis. Furthermore, we observed smaller epididymal adipocyte size(Fig. S1N), which is consistent with the previous report[31]. In addition, hepatic steatosis is also influenced by energy expenditure and exercise levels. However, we did not observe significant changes in energy metabolism and exercise levels in aADM2-tg mice (Supporting Information Fig. S2A−S2C). These results indicated that adipose ADM2 improved 8-week HFD-induced NAFLD through inhibition of hepatic *de novo* lipogenesis.

3.2. *ADM2 decreases adipose and plasma ceramide levels*

Using lipid metabolomics, we examined the lipid profiles in epididymal WAT (eWAT) (Supporting Information Fig. S3A) to identify novel lipid mediators regulated by adipose ADM2 in the aADM2-tg mice placed on an HFD for 8 weeks. Partial least squares discriminant analysis (PLS-DA) indicated that the eWAT of aADM2-tg mice had a distinct lipid metabolic pattern compared with WT mice (Fig. 2A). Analysis using the variable importance in projection (VIP) score identified that ceramides were among the top compounds that accounted for the metabolomic differences between groups (Fig. 2B).

The relative abundance of C16:0, C18:0, C24:0, and C24:1 ceramide was decreased in eWAT of aADM2-tg mice (Fig. 2C), with C14:0, C16:0, and C24:1 dihydroceramide also being decreased (Fig. 2D). In addition to eWAT, the lipid metabolomics in the subcutaneous WAT (scWAT) and plasma of aADM2-tg mice also displayed a distinct lipid metabolic pattern compared with WT mice, with marked decreases in the relative levels of C16:0, C18:0, C24:0, and C24:1 ceramide (Fig. 2E and G), decreases in C16:0, C18:0, and C24:1 dihydroceramide in scWAT (Fig. 2F), and decreases in C16:0, C24:0, and C24:1 dihydroceramide in plasma (Fig. 2H).

Furthermore, we evaluated the lipid metabolism in the liver. In contrast to the adipose tissue and plasma, the relative levels of ceramides and dihydroceramides in the liver were not decreased obviously (Fig. 2I and J). We also quantified sphingomyelin metabolisms in the above mentioned tissues, and the majority of sphingomyelin species was not altered, or even with C16 sphingomyelin was increased only in eWAT (Fig. S3B−S3E). We also observed a significantly increased level of sphingosine in the eWAT of aADM2-tg mice (Fig. 2K). These results indicated that adipose ADM2 decreased the levels of ceramide in eWAT, scWAT, and plasma, but not obviously in the liver.

3.3. *ADM2 decreased adipocyte-derived ceramide levels*

To further investigate whether lipid improvement in the liver of aADM2-tg mice may be associated with decreased adipose ceramide, we isolated primary adipocytes from the adipose tissue of mice and incubated them with ADM2; then, the conditioned medium from this culture was transferred to primary hepatocytes (Fig. 3A). We found that ceramide levels in adipocytes and conditioned medium treated with ADM2 was downregulated (Fig. 3B and C). The mRNA expression of genes involved in fatty acid transport and anabolism (*Srebp1*, *Cidea*, *Cd36*, *Fabp1*, *Fasn*, and *Scd1*) and the lipid-droplet coat (*Plin2*) were all substantially reduced in primary hepatocytes after incubation with conditioned medium from ADM2-treated adipocytes (Fig. 3D), while the mRNA expression of genes involved in fatty acid β-oxidation, such as *Acox2*, *Acsl1*, and *Acaa1a* was moderately elevated in primary hepatocytes after incubation with conditioned medium from ADM2-treated adipocytes (Fig. 3E). These results indicated that ADM2 directly decreased the levels of ceramide in adipocytes.

3.4. *Ceramides of different chain lengths stimulate gene expression associated with lipid production in primary liver cells*

It has been reported that ceramide species of different chain lengths can promote specific lipotoxicity[41]. We hence used a short-chain and three long-chain ceramides to directly stimulate primary hepatocytes. As shown, we found that the short-chain (C6:0 cer) and three long-chain ceramides (C16:0 cer, C18:0 cer, and C24:1 cer) could promote liver lipid synthesis (Fig. 4A); specifically, the mRNA expression levels for *Srebp1*, *Cidea*, and *Cd36* were significantly up-regulated. Treatment with C6:0, C16:0, and C18:0 ceramides also increased the mRNA expression levels for *Fabp1*, *Fabp4, Fasn,* and *Scd1* (Fig. 4A). We performed immunofluorescence staining experiments in parallel and found that, compared with the hepatocytes treated only with the vehicle, levels of SREBP1 protein, an intracellular promoter of lipid synthesis, were significantly increased in hepatocytes treated with different chain lengths of ceramides (Fig. 4B). We also tested the triglyceride levels in primary hepatocytes and observed a similar upward trend (Fig. 4C). These results suggest that ceramides of various different chain lengths directly and significantly promoted lipid synthesis in the liver.

3.5. *Administration of ceramide reversed the protective effect of ADM2 on NAFLD*

To further investigate whether decreased plasma ceramide levels are necessary for the decreased lipid accumulation in the liver of aADM2-tg mice, we administered HFD-fed aADM2-tg mice with C16:0 ceramide for 8 weeks (Fig. 5A). The decreased lipid accumulation and F4/80 within the liver by ADM2 administration was abolished after administration of ceramide, assessed by oil red O and H&E staining of liver sections (Fig. 5B). This was accompanied by the increased histological assessment of NAS (Fig. 5C−F). Body weight and liver weight ratio increased after administration of ceramide (Supporting Information Fig. S4A and S4B). Furthermore, both hepatic and plasma triglyceride and cholesterol levels were reversed after C16:0 administration (Fig. 5G, H and Fig. S4C and S4D). The decreased plasma levels of ALT and AST in aADM2-tg mice were abolished after C16:0 administration

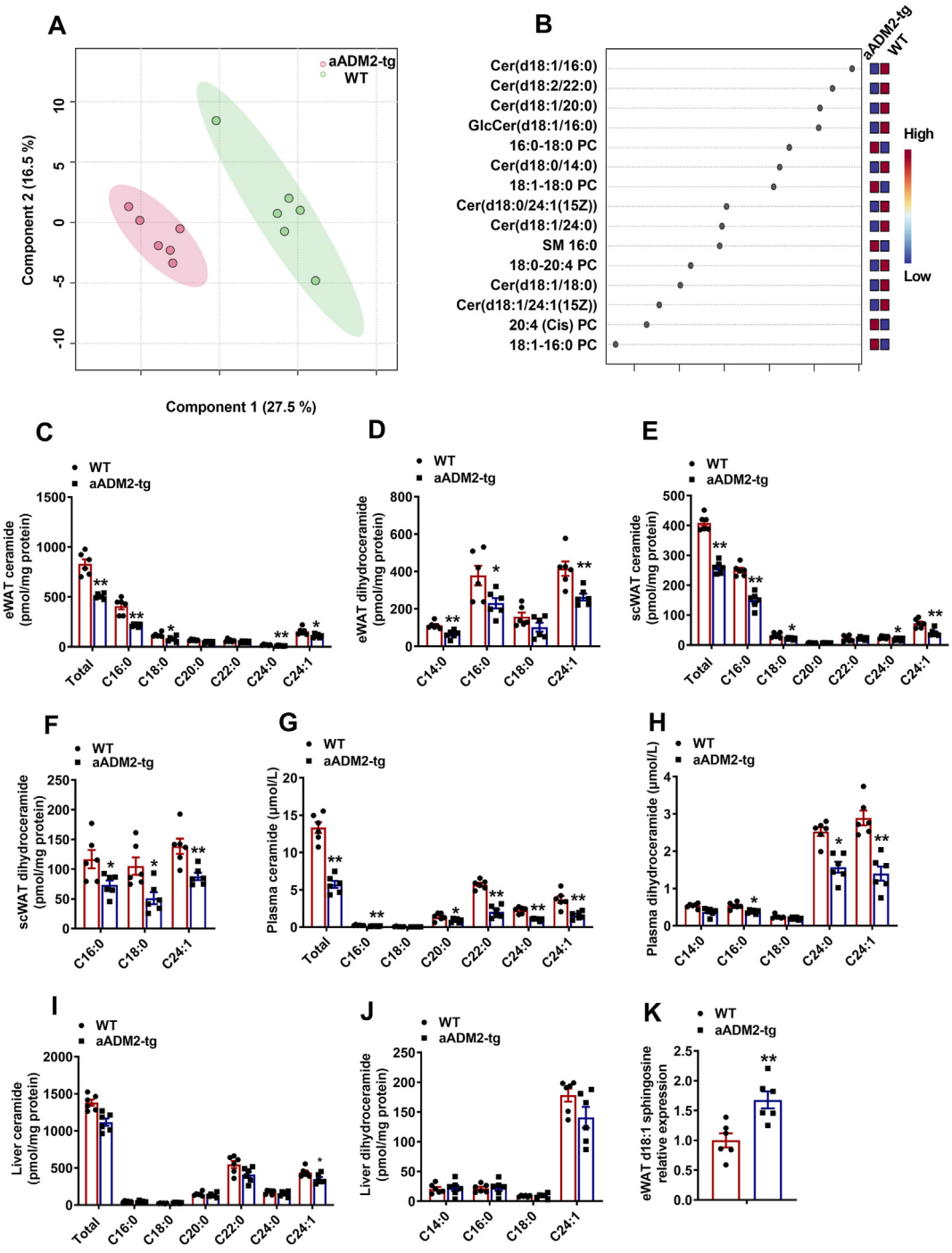

Figure 2 ADM2 decreased Adipose and plasma Ceramide levels. WT and aADM2-tg mice were fed an HFD for 8 weeks. (A) PLS-DA analysis of the metabolomics contained in eWAT ($n = 6$). (B) VIP plot identified by PLS-DA displays the top 15 most important metabolites in eWAT ($n = 6$). (C−J) HPLC−MS/MS analysis of the different species of ceramide and dihydroceramide levels in eWAT (C, D), scWAT (E, F), plasma (G, H), and liver (I, J) ($n = 6$). (K) D18:1 sphingosine level in eWAT ($n = 6$). All data are presented as the mean ± SEM. Two-tailed Student's *t*-test (D, F, K) and Mann−Whitney U test (C, E, G−J): $*P < 0.05$, $**P < 0.01$ compared to WT mice.

(Fig. 5I and J). Ceramide concentration in plasma and eWAT was upregulated after the administration of ceramide (Fig. S4E and S4F).

Furthermore, the mRNA expression levels for genes involved in fatty acid transport and anabolism (*Srebp1*, *Cidea*, *Cd36*, *Fabp1*, *Fabp4*, *Fasn*, *Scd1*, and *Elovl6*), triglyceride synthesis (*Dgat2*), and the lipid-droplet coat (*Plin2*) were all substantially elevated after C16:0 administration (Fig. 5K). By contrast, the mRNA expression levels for genes involved in fatty acid β-oxidation, such as *Acox1*, *Acsl1*, and *Acaa1a* were only moderately reduced after the administration of ceramide (Fig. 5L). In addition, decreased expression levels of inflammatory cytokines, such as *Tnfa*, *Ccl2*, and *F4/80*, the

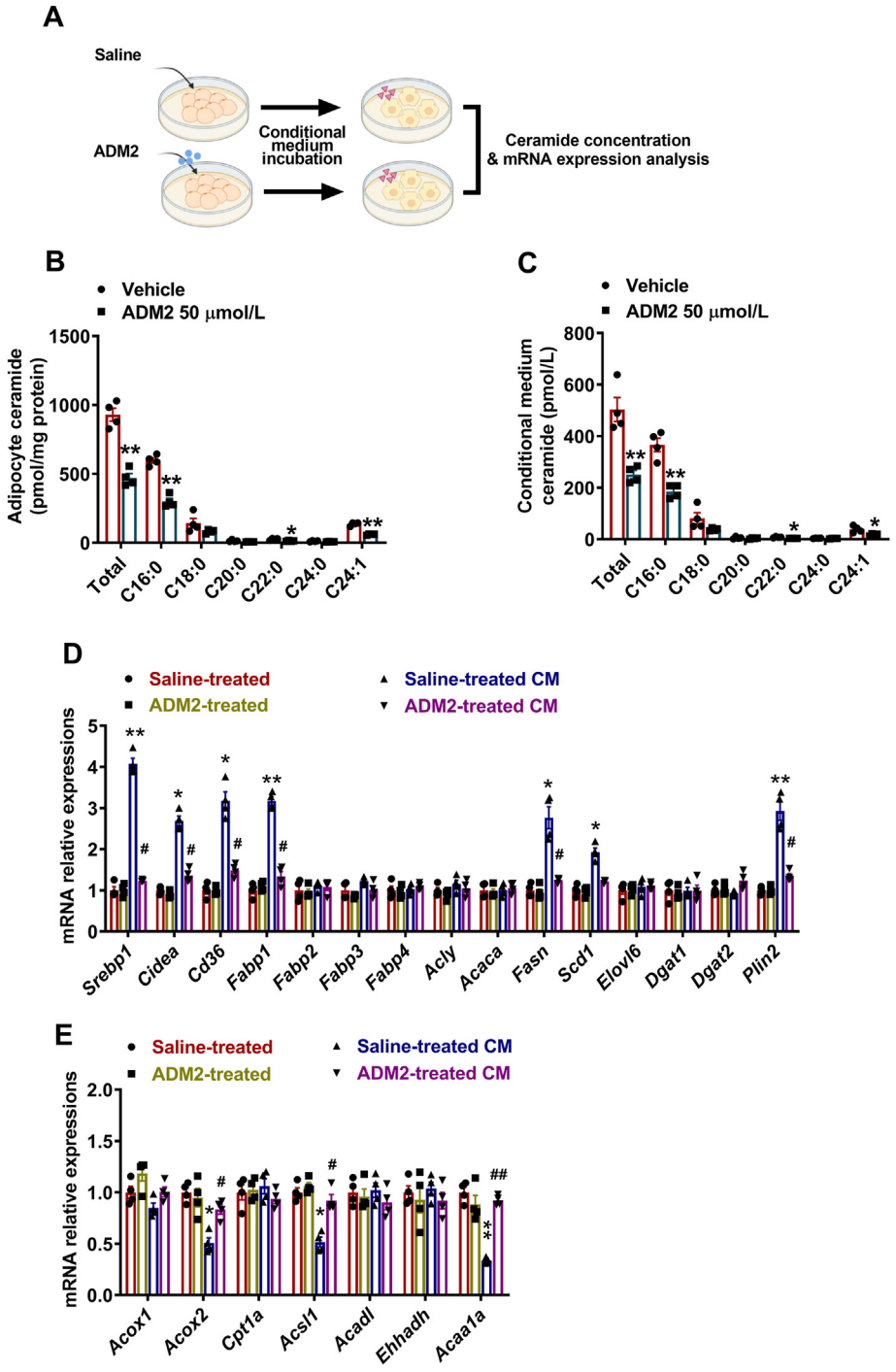

Figure 3 ADM2 decreased adipocyte-derived ceramide levels. Primary mouse adipocytes were isolated and incubated with primary hepatic cells for 12 h. (A) Conditioned medium (CM) from adipocytes incubation with primary hepatic cells. (B) Ceramide levels of ADM2-administrated primary adipocytes ($n = 4$). (C) Ceramide levels of conditioned medium ($n = 4$). (D) Hepatic expression of mRNAs encoding hepatic fatty acid transport and lipogenesis-related genes. (E) Hepatic expression of mRNAs encoding hepatic fatty acid β-oxidation-related genes from adipocyte-derived CM incubated with primary hepatic cells ($n = 4$). All data are presented as the mean ± SEM. Mann−Whitney U test (B, C), One-way ANOVA with Tukey's *post hoc* test (D, E): $^{*}P < 0.05$, $^{**}P < 0.01$ compared to vehicle. $^{\#}P < 0.05$, $^{\#\#}P < 0.01$ compared to saline-treated CM.

immunohistochemical staining of F4/80 positive cells were reversed in aADM2-tg + ceramide mice as compared to the aADM2-tg + Saline group (Fig. 5M and Fig. S4G). These results indicated that administration of ceramide reversed the protective effect of ADM2 on NAFLD.

3.6. Activation of adipocyte HIF2α mediates ADM2-induced ACER2 expression

We further explored the mechanisms responsible for the ADM2-induced reduction of adipose ceramide levels. The mRNA

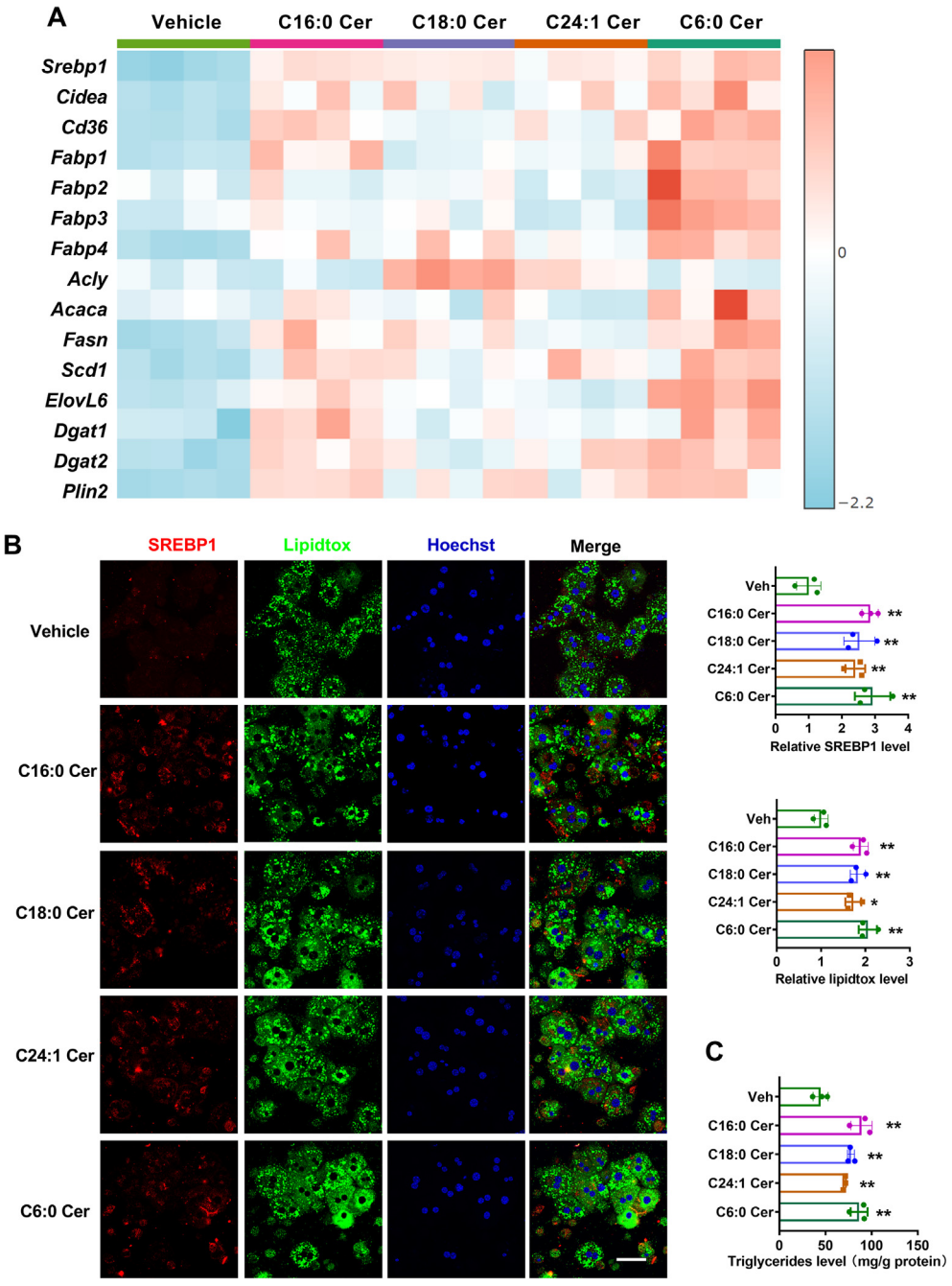

Figure 4 Ceramides of different chain lengths stimulate gene expression for lipid production in primary liver cells. Primary mouse hepatocytes were isolated and given different chain-length ceramides (C6:0, C16:0, C18:0, and C24:1 ceramide, 25 μmol/L) for 24 h. (A) Heatmap of hepatic expression of mRNAs encoded by hepatic fatty acid transport and lipogenesis-related genes ($n = 4$). (B) Immunofluorescence staining of lipid regulatory protein SREBP1 in primary hepatocytes ($n = 3$). (C) Triglycerides level in primary hepatocytes ($n = 3$). All data are presented as the means ± SEM. One-way ANOVA with Tukey's *post hoc* test (B, C), $^{*}P < 0.05$, $^{**}P < 0.01$ compared to vehicle.

expression of sphingolipid metabolic genes was examined in the eWAT of aADM2-tg mice. Among all the detected genes, the mRNA levels for *Acer2* were higher in the eWAT of aADM2-tg mice than in WT mice (Fig. 6A–C). The protein levels for ACER2 were also increased in the eWAT of HFD-treated aADM2-tg mice (Fig. 6D). The hepatic mRNA levels of sphingolipid metabolic genes remained unchanged (Supporting Information Fig. S5A–S5C). *Acer2*, which encodes a key enzyme that hydrolyzes ceramides to sphingosines and free fatty acids in alkaline conditions, was identified as a novel target gene of HIF2α, which triggers ceramide catabolism[18].

Based on GO and KEGG pathway enrichment analysis (Fig. S5D), we found that GO term of response to hypoxia pathways was significantly enriched, several hypoxia-related signaling pathways were also significantly enriched, including the PI3k–Akt signaling pathway[42,43], the cAMP signaling pathway[44,45], and the Wnt signal pathway[46]. Furthermore, we found that the HIF2 target gene pathway, and the VEGF

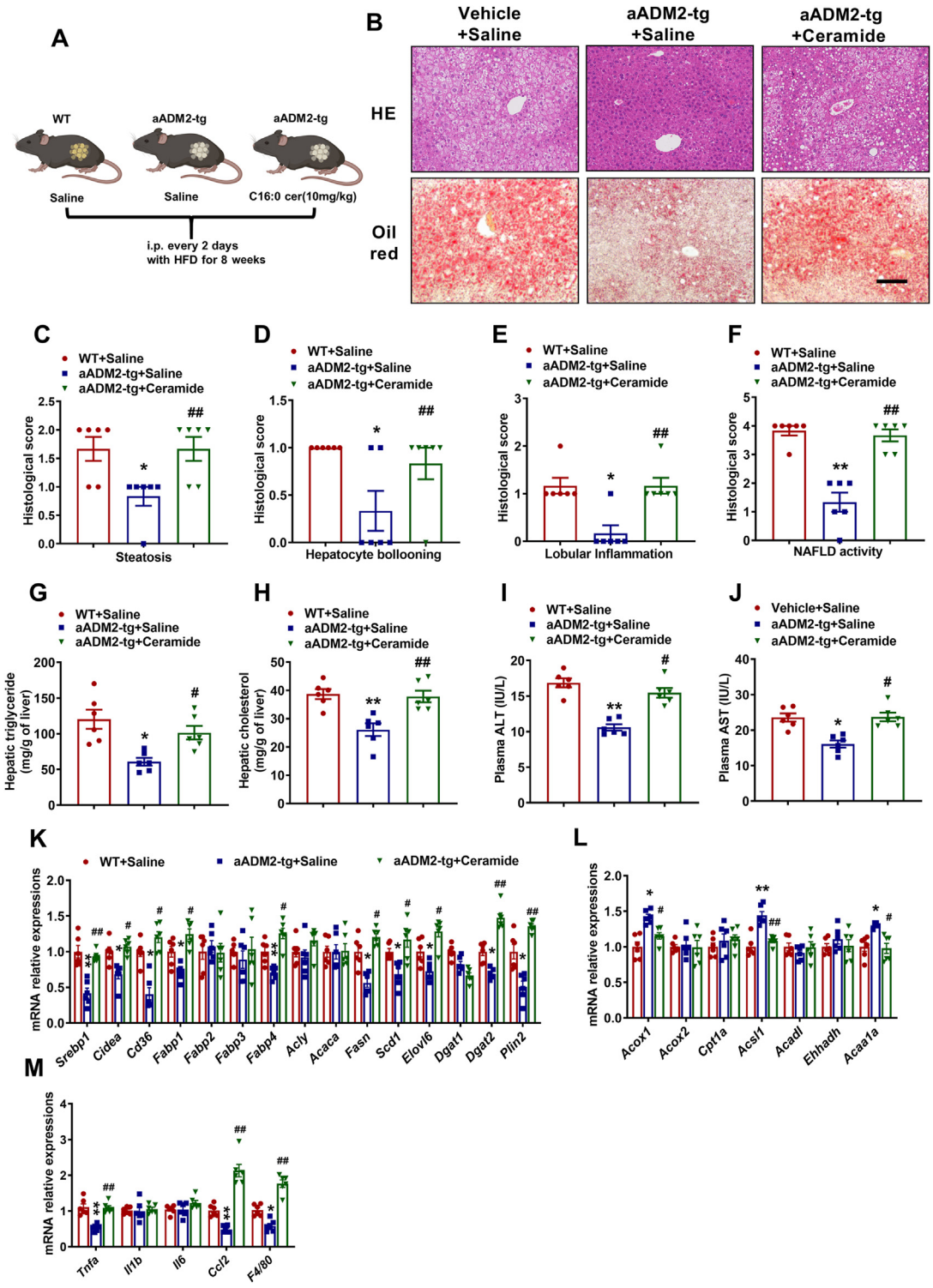

Figure 5 Administration of ceramide reversed the protective effects of ADM2 on NAFLD. Wild-type or aADM2-tg mice were given vehicle or C16:0 ceramide (10 mg/kg body weight) with HFD for 8 weeks. (A) The experimental scheme. (B) H&E and oil red O staining of representative liver sections ($n = 6$), Scale bars, 100 μm. (C) Histological scoring for steatosis ($n = 6$). (D) Histological scoring for hepatocellular ballooning ($n = 6$). (E) Histological scoring for hepatocellular inflammation ($n = 6$). (F) Histological scoring ($n = 6$). (G) Hepatic triglyceride content of mice ($n = 6$). (H) Hepatic cholesterol content of mice. (I) Plasma level of ALT. (J) Plasma level of AST. (K) Hepatic expression of mRNAs encoding hepatic fatty acid transport and lipogenesis-related genes. (L) Hepatic expression of mRNAs encoding hepatic fatty acid β-oxidation-related genes. (M) Hepatic expression of mRNAs encoding inflammatory cytokines. All data are presented as the mean ± SEM. Kruskal−Wallis test (C−F, K−M), One-way ANOVA with Tukey's *post hoc* test (G−J): $^{*}P < 0.05$, $^{**}P < 0.01$ compared to WT + Saline mice; $^{\#}P < 0.05$, $^{\#\#}P < 0.01$ compared to aADM2-tg + Saline mice.

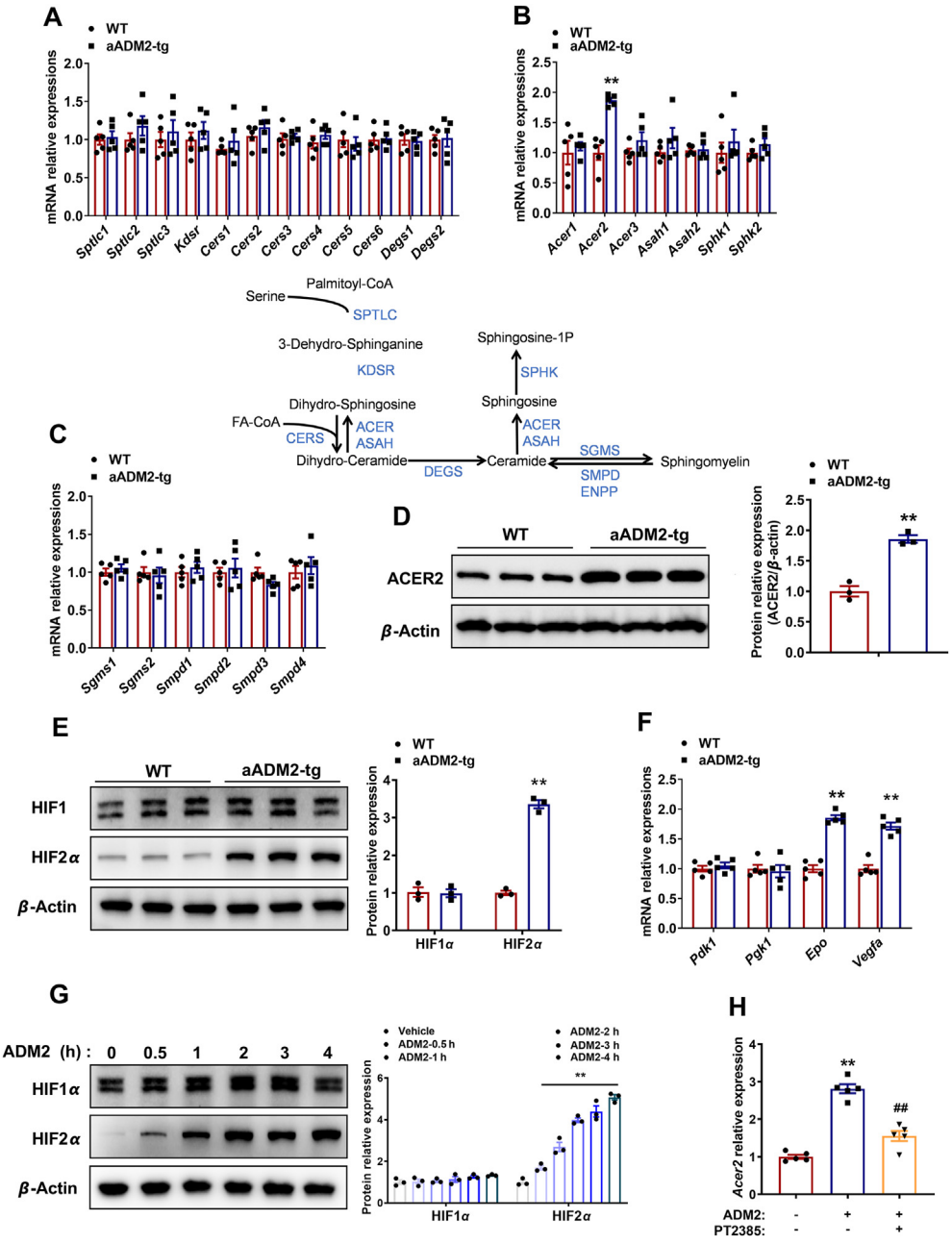

Figure 6 ADM2 decreased adipocyte-derived ceramide levels. WT and aADM2-tg mice were fed with HFD for 8 weeks. (A−C) qPCR analysis of genes involved in ceramide metabolisms in eWAT ($n = 6$). (D) Western blot analysis of ACER2 protein levels in eWAT ($n = 3$). (E) Western blot analysis of HIF1α and HIF2α protein levels in eWAT ($n = 3$). (F) qPCR analysis of HIF1α and HIF2α's target genes in eWAT ($n = 6$). (G) Western blot analysis of HIF1α and HIF2α protein levels in the differentiated 3T3-L1 adipocytes treated with ADM2 ($n = 3$). (H) Differentiated 3T3-L1 adipocytes were pretreated with PT2385 (50 nmol/L) for 0.5 h respectively, then were treated with PA (400 μmol/L) for 8 h after being given ADM2 (50 nmol/L) for 1.5 h qPCR analysis of *Acer2* in the differentiated 3T3-L1 adipocytes. All data are presented as the mean ± SEM. Mann−Whitney U test (A−C, F, G), Two-tailed Student's *t*-test (D, E), and One-way ANOVA with Tukey's *post hoc* test (H): $^{**}P < 0.01$ compared to the WT mice; $^{\#\#}P < 0.01$ compared to ADM2-treatment only group.

signaling pathway, were both also significantly enriched. These results indicated that ADM2-induced HIF2α activation may be responsible for the increase in ACER2 expression.

To explore whether ADM2 activates adipose ACER2 expression through HIF2α activation, HIF2α levels were examined in the eWAT of aADM2-tg mice. Although the mRNA levels for *Hif2α* were not significantly changed in the eWAT of aADM2-tg mice (Fig. S5E), the protein levels of HIF2α and its target genes were markedly increased (Fig. 6E and F). Since HIF2α is closely related in structure to HIF1α, we also checked the expression of HIF1α. The adipose protein levels and its target genes of HIF1α were not changed in aADM2-tg mice (Fig. 6E and F). The protein levels of HIF1α and HIF2α were also examined *in vitro*. Administration of ADM2 markedly increased the protein levels of

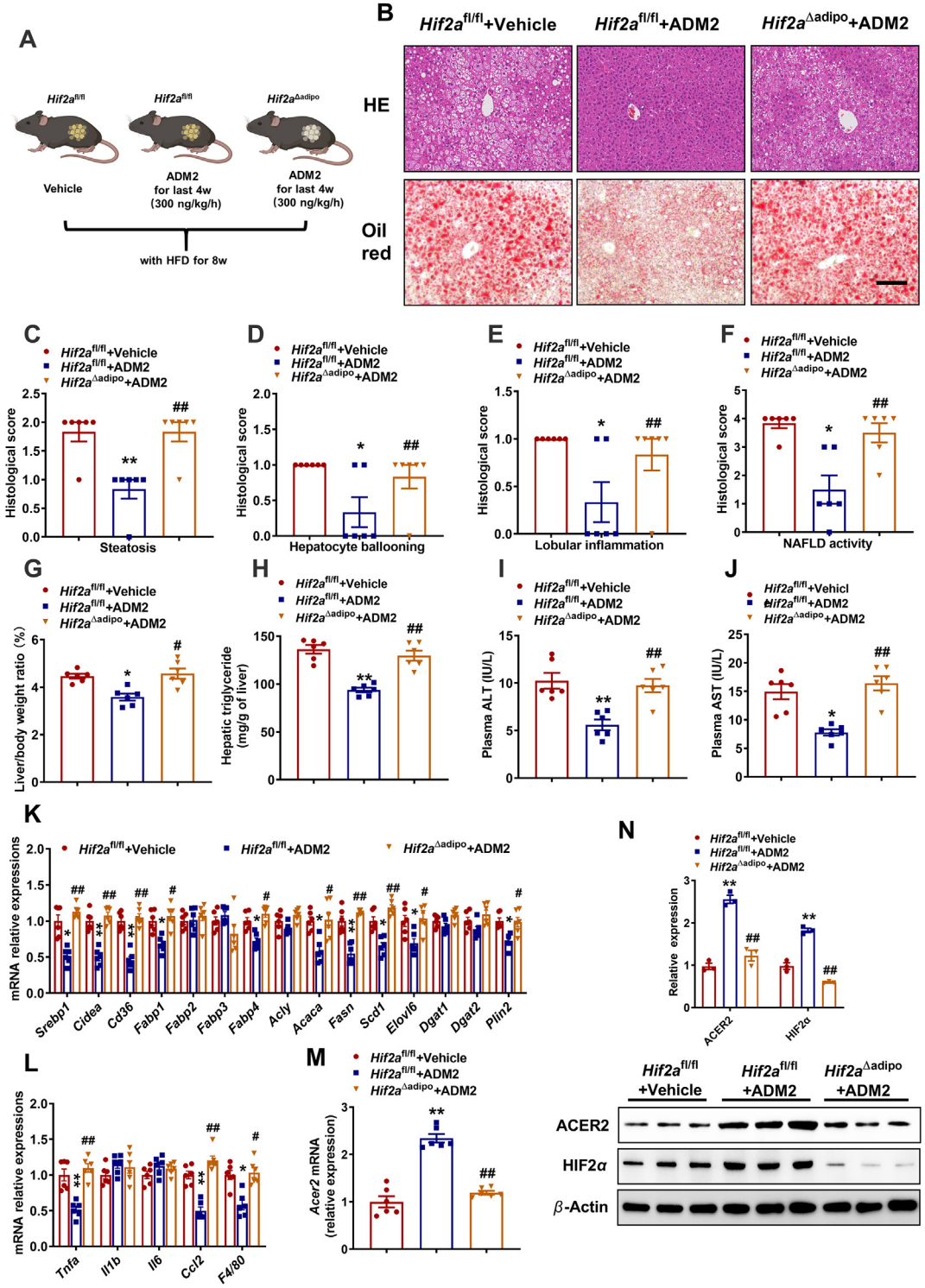

Figure 7 Adipose specific HIF2α knockout reversed the protective effect of ADM2 on NAFLD. *Hif2a*$^{fl/fl}$ and *Hif2a*$^{\Delta Adipo}$ mice were fed an HFD for 8 weeks. Adipocyte-specific HIF2α knockout (*Hif2a*$^{\Delta Adipo}$) mice were treated with HFD for 8 weeks and given ADM2 *via* an osmotic mini-pump. (A) The experimental scheme. (B) H&E and oil red O staining of representative liver sections ($n = 6$), Scale bars, 100 μm. (C) Histological scoring for steatosis ($n = 6$). (D) Histological scoring for hepatocellular ballooning ($n = 6$). (E) Histological scoring for hepatocellular inflammation ($n = 6$). (F) Histological scoring ($n = 6$). (G) Liver and body weight ratio of mice ($n = 6$). (H) Hepatic triglyceride level ($n = 6$). (I) Plasma level of ALT. (J) Plasma level of AST. (K) Hepatic expression of mRNAs encoding hepatic fatty acid transport and lipogenesis-related genes. (L) Hepatic expression of mRNAs encoding inflammatory cytokines. (M) mRNA level of *Acer2* in eWAT ($n = 6$). (N) Western blot analysis of ACER2 and HIF2α protein levels in eWAT ($n = 3$). All data are presented as the mean ± SEM. Kruskal−Wallis test (C−F, I, K, L, N), One-way ANOVA with Tukey's *post hoc* test (G, H, J, M): $^{**}P < 0.01$ compared to *Hif2a*$^{fl/fl}$ + Vehicle mice. $^{\#\#}P < 0.01$ compared to *Hif2a*$^{fl/fl}$ + ADM2 mice.

HIF2α and unchanged levels of HIF1α in adipocytes (Fig. 6G). However, *Hif2α* mRNA levels remained unchanged in ADM2-treated adipocytes (Fig. S5F). Western blotting and immunofluorescence staining experiments further revealed that ADM2 increased both the protein levels and the nuclear distribution of HIF2α in adipocytes (Fig. S5G and S5H). The ADM2-induced increase of ACER2 expression was reversed by treatment with PT2385(a HIF2α and β dimerization inhibitor) (Fig. 6H).

3.7. Adipocyte ADM2 mediates the protection of NAFLD in an adipocyte HIF2α-dependent manner

To further explore whether adipocyte HIF2α was involved in ADM2-induced inhibition of NAFLD, adipocyte-specific HIF2α knockout ($Hif2a^{\Delta Adipo}$) mice were treated with HFD for 8 weeks and then supplemented with ADM2 delivered *via* an osmotic mini-pump (Fig. 7A). We validated the tissue-specific knockout efficiency of HIF2α in the knockout mice, and the results showed that HIF2α was specifically knocked out in the adipose tissue and with high efficiency (Supporting Information Fig. S6A and S6B). The body weight of mice was slightly reversed after a 8-week-HFD treatment (Fig. S6C). Decreased lipid accumulation was observed after ADM2 treatment *via* oil red O and H&E staining of liver sections, which was abolished in the ADM2-treated $Hif2a^{\Delta}$Adipo mice (Fig. 7B−F). ADM2 decreased the hepatic liver/body weight ratio and triglyceride content in $Hif2a^{fl/fl}$ mice, but not in the $Hif2a^{\Delta Adipo}$ mice (Fig. 7G and H). The plasma levels of ALT and AST were also decreased in the $Hif2a^{fl/fl}$ mice after ADM2 treatment, which was absent in the $Hif2a^{\Delta Adipo}$ mice (Fig. 7I and J). The plasma levels of triglyceride and cholesterol, and hepatic cholesterol were also decreased in aADM2-tg mice; however, these decreases were not observed in $Hif2a^{\Delta Adipo}$ mice (Fig. S6D−S6F). Ceramide concentrations in the plasma and eWAT were upregulated in the $Hif2a^{\Delta Adipo}$ mice (Fig. S6G and S6H), while sphingosine level was downregulated in the eWAT of $Hif2a^{\Delta Adipo}$ mice (Fig. S6I).

Furthermore, the mRNA expression levels for genes involved in fatty acid transport and anabolism (*Srebp1*, *Cidea*, *Cd36*, *Fabp1*, *Fabp4*, *Acaca*, *Fasn*, *Scd1*, and *Elovl6*), and the lipid-droplet coat (*Plin2*) were all reduced in $Hif2a^{fl/fl}$ mice + ADM2 mice, compared to controls, but these changes were not detected in $Hif2a^{\Delta Adipo}$ + ADM2 mice (Fig. 7K). Moreover, the expression levels of inflammatory cytokines, such as *Tnfa*, *Ccl2*, and *F4/80*, the immunohistochemical staining of F4/80 positive cells, were significantly lower in $Hif2a^{fl/fl}$ + ADM2 mice compared to controls, however, these differences were not observed in $Hif2a^{\Delta Adipo}$ + ADM2 mice (Fig. 7L and Fig. S6J). The expression of *Acer2* was also examined in the ADM2-treated $Hif2a^{fl/fl}$ and $Hif2a^{\Delta Adipo}$ mice. The adipose *Acer2* mRNA and protein levels were upregulated by ADM2 in the $Hif2a^{fl/fl}$ mice, but not in $Hif2a^{\Delta Adipo}$ mice (Fig. 7M and N). These results indicate that ADM2 induced adipose ACER2 expression and was protective against NAFLD in a HIF2α-dependent manner.

3.8. Adipocyte ADM2 mediates the protection of NAFLD in an adipocyte ACER2-dependent manner

We used lentiviral shRNA vectors to achieve adipose-specific ACER2 knockdown *via in situ* injections into the visceral adipose tissue of mice, and the knockout efficiency was validated (Supporting Information Fig. S7A and S7B). Decreased lipid accumulation was observed after ADM2 treatment *via* oil red O and H&E staining of liver sections, but these phenotypes were not observed in LV-ShACER2-treated aADM2-tg mice (Fig. S7C−S7G). ADM2 decreased the hepatic liver/body weight ratio and triglyceride content in the aADM2-tg mice, but not in LV-ShACER2-treated aADM2-tg mice (Fig. S7H and S7I). The downregulation of ceramide concentrations in both plasma and eWAT was abolished in the $Hif2a^{\Delta Adipo}$ mice and the LV-ShACER2-treated aADM2-tg mice (Fig. S7J and S7K). Furthermore, the mRNA expression of genes involved in fatty acid transport, anabolism, and inflammatory cytokines in the LV-ShACER2-treated aADM2-tg mice was reminiscent of the profiles for such genes measured in $Hif2a^{\Delta Adipo}$ mice (Fig. S7L and S7M). These results indicated that ADM2 induced adipose ACER2 expression and protected NAFLD in a HIF2α-ACER2-dependent manner.

4. Discussion

ADM2 has been reported to increase the content of intracellular cAMP and mediate a variety of biological effects such as myocardial contraction, vasodilatation, inhibition of vascular calcification, regulating cell proliferation, hypertrophy, migration, and apoptosis[47]. Although our previous studies have shown the importance of adipose ADM2 in lipid metabolism, whether ADM2 has a protective effect on NAFLD development is still unknown. In the present study, we report that adipose ADM2 promotes ceramide catabolism and subsequently improves NAFLD.

Hepatic steatosis is influenced by liver lipid export, and lipid synthesis, in addition to fat function[48]. We discovered that the liver and body weight ratios were decreased in aADM2-tg mice, and the hepatic triglyceride and total cholesterol contents were decreased in aADM2-tg mice compared to controls, indicating improved hepatic function. Perhaps due to the different construction of overexpressing promoters in mouse strains, some results may not be completely consistent with previous studies[31], such as energy expenditure, plasma cholesterol, and plasma triglycerides. In aADM2-tg mice, we found that there was no change in food intake, exercise levels, or liver lipid output, while lipid synthesis was inhibited. This suggests that there are some other regulatory mechanisms improving liver lipid metabolism.

"Ceramide reduction therapies", such as inhibiting ceramide biosynthesis or catalyzing ceramide degradation in rodents, have been touted as a potential strategy to ameliorate metabolic disorders[13]. Elevated circulating ceramides are observed in patients with type 2 diabetes and these levels correlate with the severity of metabolic disease[49]. Further mechanistic studies have shown that ADM2 can activate the adipocyte HIF2α signaling pathway and up-regulate ACER2 expression, promote ceramide catabolism, and reduce ceramide levels. Adipocyte HIF2α deficiency exacerbated western-diet-induced dyslipidemia by increasing adipose ceramide levels, which is dependent on the effect of the HIF2α-ACER2-ceramide axis in dyslipidemia development[18]. This is consistent with our findings that show that the deletion of adipocyte HIF2α resulted in enhanced WAT dysfunction in the obese condition, increased serum ceramide levels, and ectopic fat accumulation in the liver. It is also reported that overexpression of acid ceramidase within adipose tissue prevents hepatic steatosis and insulin resistance. The prominent cross-talk between the liver and adipose tissue highlights the importance of equilibration of sphingolipids between the two tissues[49].

In previous studies, exogenous administration of C16:0 ceramide was found to directly promote the expression of *Srebp1c* in the liver, leading to the exacerbation of NAFLD symptoms[50]; At the same time, ceramides can directly induce hepatic ER stress, and indirectly regulate hepatic gluconeogenesis, and aggravate hepatic lipid accumulation[51]. Based on our data, we found a significant decrease in plasma ceramides. Although we did not observe a significant decrease in liver ceramides, the liver was enriched with a large amount of flowing blood and had overall lower levels of ceramide circulation. Continuously decreasing plasma ceramides could reduce overall lipid accumulation in liver cells. There may also be membrane receptors on the surface of liver cells that sense changes with plasma ceramides. Decreased plasma ceramides can reduce stimulation to liver cells or improve the conformation of liver cell membranes, thereby reducing liver lipid accumulation. Which is still worth further exploration. Therefore, our study confirms the importance of ceramides in the pathogenesis of diet-induced NAFLD. Specifically, the rapid release of ceramide from adipocytes into the portal circulation for delivery to the liver exerts an important effect on the progression of fatty liver disease.

Low plasma level of ADM2[25], indicates that ADM2 may act in an autocrine or paracrine manner, regulating organ perfusion and hormone secretion[22]. According to a recent article[24], Babin'group found that adrenomedullin 2/intermedin is a slow off-rate, long-acting endogenous agonist of the adrenomedullin2 G protein-coupled receptor. ADM2 belongs to the CGRP superfamily of peptides, usually used as a signaling peptide to exert regulatory effects on the cell surface. The common receptors of the CGRP family are calcitonin receptor-like receptor/receptor activity modifying protein (CRLR/RAMP) complexes[22].

We conducted a transcriptomic analysis of the adipose tissue from ADM2-overexpressing mice and found that ADM2 treatment could significantly activate hypoxia-induced signaling (Fig. S5D). Based on GO and KEGG pathway enrichment, we found that several hypoxia-related signaling pathways were activated (Fig. S5D): (1) The PI3k−Akt signaling pathway has been shown to be related to HIF2 activation[42,43]; (2) ADM2 is well known to increase the content of intracellular cAMP and mediates a variety of biological effects[47]. ADM2/IMD1−47 exerts a direct, positive inotropic effect through the CGRP receptor−cAMP pathway in the endothelium[52]. Garcia and colleagues found that cAMP-response element binding protein (CBP) has an impact on HIF2α-specific affinity regulation for HIF1α. They found that CBP can specifically participate with HIF2 as a major co-activator of HIF2α acetylation, assisting in mediating their activation of the target gene Epo[45]. To promote adipogenic conversion and prevent apoptosis of mature adipocytes, an early increase in cAMP levels stimulates PKA in preadipocytes, which phosphorylates and activates the nuclear basic leucine zipper transcription factor cAMP-response element-binding (CREB) protein and members of the ATF family[53]. Furthermore, it was demonstrated that the lysine acetyltransferase CBP is required for efficient Epo induction during hypoxia[45]. Thus, we speculate that ADM2 could activate the cAMP signaling pathway to stabilize HIF2α protein level *via* CBP; (3) β-catenin, downstream of the Wnt signal pathway, could stabilize HIF2α through a lncRNA signaling pathway[46]. Furthermore, the protection on NAFLD progression mediated by ADM2 administration was abolished with adipocyte HIF2α deficiency, indicating that ADM2 improves NAFLD through modulating adipose ceramide generation in an adipocyte HIF2α-dependent manner. The specific, underlying mechanism requires further investigation.

There are several limitations in this study. We have not explored other tissues and organs besides the liver; how does ADM2 regulate the activation of hypoxia-inducible factors and why does it have a unique effect on HIF2α? These are all issues that need to be clarified. Elevated adipocyte-derived ceramide levels and ectopic lipid deposition both represent important pathogenic factors for NAFLD. Herein, we adopted the adipose-specific ADM2 transgenic (aADM2-tg) mice to study the role and dissect the mechanisms of ADM2 in adipose ceramide generation and NAFLD development. Our research suggests that ADM2 could exert a localized effect in adipose tissue by activating adipocyte HIF2α to promote ACER2-dependent ceramide catabolism and reduce liver lipid accumulation. Our results suggest that ADM2 and adipose-derived ceramide are potential therapeutic candidates for NAFLD and related metabolic disorders. However, there are still several scientific questions that need to be addressed, such as whether cells have more precise regulatory mechanisms for perceiving small changes in ceramides, is there a membrane protein receptor for ceramide on the surface of liver cells to regulate lipid changes? At the cellular level *in vitro*, the precise regulation of ceramides and their tissue-specific functions is well understood, while we are only beginning to understand their biological functions in disease models *in vivo*. Studying the underlying role of these lipids in cellular function will be crucial for developing new therapies and improving our understanding of the causes of metabolic disorders.

5. Conclusions

The above results confirm that ADM2 can act as a protective peptide to exert metabolic regulation in adipose tissue, by stabilizing the expression of HIF-2α protein, activating the downstream target gene *Acer2* of HIF-2α, to regulate ceramide catabolism in adipose tissue, and improving simple fatty liver. This study reveals the important role of the adipose-derived ADM2−HIF-2α−ceramide axis in the occurrence and development of NAFLD, providing new strategies and potential drug targets for the treatment of NAFLD.

Acknowledgments

This work was supported by the National Key Research and Development Program of China (Nos. 2020YFA0803801, 2022YFA0806400, and 2018YFA0800701), the National Natural Science Foundation of China (Nos. 81921001 and 32200949), the project funded by China Postdoctoral Science Foundation (BX20220021, China). Xin Du and Julian Heng (Remotely Consulting, Australia) provided professional English-language editing of this article (Certificate No. 2Tv2Ry7I).

Author contributions

Pengcheng Wang: Writing − review & editing, Writing − original draft, Visualization, Methodology, Investigation, Funding acquisition, Formal analysis, Data curation. Song-Yang Zhang: Writing − original draft, Data curation, Conceptualization. YongQiang Dong: Writing − review & editing, Validation, Formal analysis, Data curation. Guangyi Zeng: Validation, Methodology, Data curation. Huiying Liu: Validation, Methodology, Investigation. Xian Wang: Writing − original draft, Supervision,

Conceptualization. Changtao Jiang: Writing − review & editing, Funding acquisition, Conceptualization. Yin Li: Writing − original draft, Supervision, Funding acquisition, Conceptualization.

Conflicts of interest

The authors declare no competing interests.

Appendix A. Supporting information

Supporting information to this article can be found online at https://doi.org/10.1016/j.apsb.2024.09.010.

References

1. Powell EE, Wong VW, Rinella M. Non-alcoholic fatty liver disease. *Lancet* 2021;**397**:2212−24.
2. Vuppalanchi R, Noureddin M, Alkhouri N, Sanyal AJ. Therapeutic pipeline in nonalcoholic steatohepatitis. *Nat Rev Gastroenterol Hepatol* 2021;**18**:373−92.
3. Francque S, Szabo G, Abdelmalek MF, Byrne CD, Cusi K, Dufour JF, et al. Nonalcoholic steatohepatitis: the role of peroxisome proliferator-activated receptors. *Nat Rev Gastroenterol Hepatol* 2021;**18**:24−39.
4. Huby T, Gautier EL. Immune cell-mediated features of non-alcoholic steatohepatitis. *Nat Rev Immunol* 2022;**22**:429−43.
5. Cotter TG, Rinella M. Nonalcoholic fatty liver disease 2020: the state of the disease. *Gastroenterology* 2020;**158**:1851−64.
6. Fan JG, Kim SU, Wong VW. New trends on obesity and NAFLD in Asia. *J Hepatol* 2017;**67**:862−73.
7. Friedman SL, Neuschwander-Tetri BA, Rinella M, Sanyal AJ. Mechanisms of NAFLD development and therapeutic strategies. *Nat Med* 2018;**24**:908−22.
8. Liu R, Li Y, Zheng Q, Ding M, Zhou H, Li X. Epigenetic modification in liver fibrosis: promising therapeutic direction with significant challenges ahead. *Acta Pharm Sin B* 2024;**14**:1009−29.
9. Jin X, Qiu T, Li L, Yu R, Chen X, Li C, et al. Pathophysiology of obesity and its associated diseases. *Acta Pharm Sin B* 2023;**13**:2403−24.
10. Van der Poorten D, Milner KL, Hui J, Hodge A, Trenell MI, Kench JG, et al. Visceral fat: a key mediator of steatohepatitis in metabolic liver disease. *Hepatology* 2008;**48**:449−57.
11. Ooi GJ, Meikle PJ, Huynh K, Earnest A, Roberts SK, Kemp W, et al. Hepatic lipidomic remodeling in severe obesity manifests with steatosis and does not evolve with non-alcoholic steatohepatitis. *J Hepatol* 2021;**75**:524−35.
12. Xie C, Yagai T, Luo Y, Liang X, Chen T, Wang Q, et al. Activation of intestinal hypoxia-inducible factor 2α during obesity contributes to hepatic steatosis. *Nat Med* 2017;**23**:1298−308.
13. Chaurasia B, Summers SA. Ceramides—lipotoxic inducers of metabolic disorders. *Trends Endocrinol Metab* 2015;**26**:538−50.
14. Nikolova-Karakashian M. Alcoholic and non-alcoholic fatty liver disease: focus on ceramide. *Adv Biol Regul* 2018;**70**:40−50.
15. Wang P, Zeng G, Yan Y, Zhang SY, Dong Y, Zhang Y, et al. Disruption of adipocyte HIF-1α improves atherosclerosis through the inhibition of ceramide generation. *Acta Pharm Sin B* 2022;**12**:1899−912.
16. Jiang C, Xie C, Li F, Zhang L, Nichols RG, Krausz KW, et al. Intestinal farnesoid X receptor signaling promotes nonalcoholic fatty liver disease. *J Clin Invest* 2015;**125**:386−402.
17. Wu Q, Sun L, Hu X, Wang X, Xu F, Chen B, et al. Suppressing the intestinal farnesoid X receptor/sphingomyelin phosphodiesterase 3 axis decreases atherosclerosis. *J Clin Invest* 2021;**131**:e142865.
18. Zhang X, Zhang Y, Wang P, Zhang SY, Dong Y, Zeng G, et al. Adipocyte hypoxia-inducible factor 2alpha suppresses atherosclerosis by promoting adipose ceramide catabolism. *Cell Metab* 2019;**30**. 937-51.e5.
19. Summers SA. The ART of lowering ceramides. *Cell Metab* 2015;**22**:195−6.
20. Chen B, Sun L, Zeng G, Shen Z, Wang K, Yin L, et al. Gut bacteria alleviate smoking-related NASH by degrading gut nicotine. *Nature* 2022;**610**:562−8.
21. Chang CL, Roh J, Hsu SYT. Intermedin, a novel calcitonin family peptide that exists in teleosts as well as in mammals: a comparison with other calcitonin/intermedin family peptides in vertebrates. *Peptides* 2004;**25**:1633−42.
22. Zhang SY, Xu MJ, Wang X. Adrenomedullin 2/intermedin: a putative drug candidate for treatment of cardiometabolic diseases. *Br J Pharmacol* 2018;**175**:1230−40.
23. Roh J, Chang CL, Bhalla A, Klein C, Hsu SYT. Intermedin is a calcitonin/calcitonin gene-related peptide family peptide acting through the calcitonin receptor-like receptor/receptor activity-modifying protein receptor complexes. *J Biol Chem* 2004;**279**:7264−74.
24. Babin KM, Karim JA, Gordon PH, Lennon J, Dickson A, Pioszak AA. Adrenomedullin 2/intermedin is a slow off-rate, long-acting endogenous agonist of the adrenomedullin2 G protein−coupled receptor. *J Biol Chem* 2023;**299**:104785.
25. Takahashi K, Kikuchi K, Maruyama Y, Urabe T, Nakajima K, Sasano H, et al. Immunocytochemical localization of adrenomedullin 2/intermedin-like immunoreactivity in human hypothalamus, heart and kidney. *Peptides* 2006;**27**:1383−9.
26. Zhang SY, Lv Y, Zhang H, Gao S, Wang T, Feng J, et al. Adrenomedullin 2 improves early obesity-induced adipose insulin resistance by inhibiting the class II major histocompatibility complex in adipocytes. *Diabetes* 2016;**65**:2342−55.
27. Zhang X, Gu L, Chen X, Wang S, Deng X, Liu K, et al. Intermedin ameliorates atherosclerosis in ApoE null mice by modifying lipid profiles. *Peptides* 2012;**37**:189−93.
28. Lv Y, Zhang S-Y, Liang X, Zhang H, Xu Z, Liu B, et al. Adrenomedullin 2 enhances beiging in white adipose tissue directly in an adipocyte-autonomous manner and indirectly through activation of M2 macrophages. *J Biol Chem* 2016;**291**:23390−402.
29. Ni X, Zhang J, Tang C, Qi Y. Intermedin/adrenomedullin2: an autocrine/paracrine factor in vascular homeostasis and disease. *Sci China Life Sci* 2014;**57**:781−9.
30. Yang JH, Jia YX, Pan CS, Zhao J, Ouyang M, Yang J, et al. Effects of intermedin(1−53) on cardiac function and ischemia/reperfusion injury in isolated rat hearts. *Biochem Biophys Res Commun* 2005;**327**:713−9.
31. Zhang H, Zhang SY, Jiang C, Li Y, Xu G, Xu MJ, et al. Intermedin/adrenomedullin 2 polypeptide promotes adipose tissue browning and reduces high-fat diet-induced obesity and insulin resistance in mice. *Int J Obes* 2016;**40**:852−60.
32. Wang ZV, Deng Y, Wang QA, Sun K, Scherer PE. Identification and characterization of a promoter cassette conferring adipocyte-specific gene expression. *Endocrinology* 2010;**151**:2933−9.
33. Eguchi J, Wang X, Yu S, Kershaw EE, Chiu PC, Dushay J, et al. Transcriptional control of adipose lipid handling by IRF4. *Cell Metab* 2011;**13**:249−59.
34. Yuan F, Zhang Q, Dong H, Xiang X, Zhang W, Zhang Y, et al. Effects of des-acyl ghrelin on insulin sensitivity and macrophage polarization in adipose tissue. *J Transl Int Med* 2021;**9**:84−97.
35. Yan Y, Wu X, Wang P, Zhang S, Sun L, Zhao Y, et al. Homocysteine promotes hepatic steatosis by activating the adipocyte lipolysis in a HIF1α−ERO1α-dependent oxidative stress manner. *Redox Biol* 2020;**37**:101742.
36. Cui A, Fan H, Zhang Y, Zhang Y, Niu D, Liu S, et al. Dexamethasone-induced Krüppel-like factor 9 expression promotes hepatic gluconeogenesis and hyperglycemia. *J Clin Invest* 2019;**129**:2266−78.
37. Zhang S-Y, Dong Y-Q, Wang P, Zhang X, Yan Y, Sun L, et al. Adipocyte-derived lysophosphatidylcholine activates adipocyte and adipose tissue macrophage Nod-like receptor protein 3 inflammasomes mediating homocysteine-induced insulin resistance. *EBioMed* 2018;**31**:202−16.
38. Rastogi A, Shasthry SM, Agarwal A, Bihari C, Jain P, Jindal A, et al. Non-alcoholic fatty liver disease—histological scoring systems: a large cohort single-center, evaluation study. *APMIS* 2017;**125**:962−73.

39. Huang DW, Sherman BT, Lempicki RA. Bioinformatics enrichment tools: paths toward the comprehensive functional analysis of large gene lists. *Nucleic Acids Res* 2009;**37**:1−13.
40. Huang DW, Sherman BT, Lempicki RA. Systematic and integrative analysis of large gene lists using DAVID bioinformatics resources. *Nat Protoc* 2009;**4**:44−57.
41. Hammerschmidt P, Bruning JC. Contribution of specific ceramides to obesity-associated metabolic diseases. *Cell Mol Life Sci* 2022;**79**:395.
42. Mohlin S, Hamidian A, von Stedingk K, Bridges E, Wigerup C, Bexell D, et al. PI3K−mTORC2 but not PI3K−mTORC1 regulates transcription of HIF2A/EPAS1 and vascularization in neuroblastoma. *Cancer Res* 2015;**75**:4617−28.
43. Joshi S, Singh AR, Zulcic M, Durden DL. A macrophage-dominant PI3K isoform controls hypoxia-induced HIF1α and HIF2α stability and tumor growth, angiogenesis, and metastasis. *Mol Cancer Res* 2014;**12**:1520−31.
44. Fox KE, Fankell DM, Erickson PF, Majka SM, Crossno Jr JT, Klemm DJ. Depletion of cAMP-response element-binding protein/ATF1 inhibits adipogenic conversion of 3T3-L1 cells ectopically expressing CCAAT/enhancer-binding protein (C/EBP) alpha, C/EBP beta, or PPAR gamma 2. *J Biol Chem* 2006;**281**:40341−53.
45. Chen R, Xu M, Hogg RT, Li J, Little B, Gerard RD, et al. The acetylase/deacetylase couple CREB-binding protein/Sirtuin 1 controls hypoxia-inducible factor 2 signaling. *J Biol Chem* 2012;**287**:30800−11.
46. Nakagawa C, Kadlera Nagaraj M, Hernandez JC, Uthay Kumar DB, Shukla V, Machida R, et al. β-CATENIN stabilizes HIF2 through lncRNA and inhibits intravenous immunoglobulin immunotherapy. *Front Immunol* 2023;**14**:1204907.
47. Li P, Sun HJ, Han Y, Wang JJ, Zhang F, Tang CS, et al. Intermedin enhances sympathetic outflow *via* receptor-mediated cAMP/PKA signaling pathway in nucleus tractus solitarii of rats. *Peptides* 2013;**47**:1−6.
48. Li B, Xiao Q, Zhao H, Zhang J, Yang C, Zou Y, et al. Schisanhenol ameliorates non-alcoholic fatty liver disease *via* inhibiting miR-802 activation of AMPK-mediated modulation of hepatic lipid metabolism. *Acta Pharm Sin B* 2024;**14**:3949−63.
49. Xia JY, Holland WL, Kusminski CM, Sun K, Sharma AX, Pearson MJ, et al. Targeted induction of ceramide degradation leads to improved systemic metabolism and reduced hepatic steatosis. *Cell Metab* 2015;**22**:266−78.
50. Xie C, Jiang C, Shi J, Gao X, Sun D, Sun L, et al. An intestinal farnesoid X receptor−ceramide signaling axis modulates hepatic gluconeogenesis in mice. *Diabetes* 2017;**66**:613−26.
51. Chiang JYL. Bile acids: regulation of synthesis. *J Lipid Res* 2009;**50**:1955−66.
52. Pires AL, Pinho M, Sena CM, Seica R, Leite-Moreira AF. Intermedin elicits a negative inotropic effect in rat papillary muscles mediated by endothelial-derived nitric oxide. *Am J Physiol Heart Circ Physiol* 2012;**302**:H1131−7.
53. Ravnskjaer K, Madiraju A, Montminy M. Role of the cAMP pathway in glucose and lipid metabolism. *Handb Exp Pharmacol* 2016;**233**:29−49.